

Time-energy distribution of photoelectron from atomic states with different magnetic quantum numbers in elliptically polarized laser fields

Jingyang Xu(徐菁阳), Li Guo(郭丽), Xin Qi(齐昕), Ronghua Lu(陆荣华), Min Zhang(张敏), Jingtao Zhang(张敬涛), and Jing Chen(陈京)

Citation: Chin. Phys. B, 2024, 33 (**9**): 093301. DOI: 10.1088/1674-1056/ad58b3
Journal homepage: http://cpb.iphy.ac.cn; http://iopscience.iop.org/cpb

What follows is a list of articles you may be interested in

Excitation and ionization of OCS molecules in strong UV and NIR laser fields

Huijun Shi(师慧军), Yang Liu(刘洋), Tian Sun(孙添), Hang Lv(吕航), and Haifeng Xu(徐海峰)
Chin. Phys. B, 2024, 33 (**7**): 073301. DOI: 10.1088/1674-1056/ad3035

Comparative study of photoionization of atomic hydrogen by solving the one- and three-dimensional time-dependent Schrödinger equations

Shun Wang(王顺), Shahab Ullah Khan, Xiao-Qing Tian(田晓庆), Hui-Bin Sun(孙慧斌), and Wei-Chao Jiang(姜维超)
Chin. Phys. B, 2021, 30 (**8**): 083301. DOI: 10.1088/1674-1056/abea85

Effect of laser polarization on strong-field ionization and fragmentation of nitrous oxide molecules

Rui Wang(王瑞), Shi-Wen Zhang(张世文), Yang Liu(刘洋), Tian Sun(孙添), Hang Lv(吕航), Hai-Feng Xu(徐海峰)
Chin. Phys. B, 2019, 28 (**5**): 053301. DOI: 10.1088/1674-1056/28/5/053301

Enhanced ionization of vibrational hot carbon disulfide molecules in strong femtosecond laser fields

Wan-Long Zuo(左万龙), Hang Lv(吕航), Hong-Jing Liang(梁红静), Shi-Min Shan(单石敏), Ri Ma(马日), Bing Yan(闫冰), Hai-Feng Xu(徐海峰)
Chin. Phys. B, 2018, 27 (**6**): 063301. DOI: 10.1088/1674-1056/27/6/063301

Ellipticity-dependent ionization/dissociation of carbon dioxide in strong laser fields

Zhang Jun-Feng (张军峰), Ma Ri (马日), Zuo Wan-Long (左万龙), Lv Hang (吕航), Huang Hong-Wei (黄红卫), Xu Hai-Feng (徐海峰), Jin Ming-Xing (金明星), Ding Da-Jun (丁大军)
Chin. Phys. B, 2015, 24 (**3**): 033302. DOI: 10.1088/1674-1056/24/3/033302

Time–energy distribution of photoelectron from atomic states with different magnetic quantum numbers in elliptically polarized laser fields

Jingyang Xu(徐菁阳)[1], Li Guo(郭丽)[1,†], Xin Qi(齐昕)[1], Ronghua Lu(陆荣华)[2], Min Zhang(张敏)[1,‡], Jingtao Zhang(张敬涛)[1], and Jing Chen(陈京)[3,4,§]

[1] *Department of Physics, Shanghai Normal University, Shanghai* 200234, *China*
[2] *Key Laboratory for Quantum Optics and Center for Cold Atom Physics, Shanghai Institute of Optics and Fine Mechanics, Chinese Academy of Sciences, Shanghai* 201800, *China*
[3] *Hefei National Research Center for Physical Sciences at the Microscale and School of Physical Sciences, University of Science and Technology of China, Hefei* 230026, *China*
[4] *Shenzhen Key Laboratory of Ultraintense Laser and Advanced Material Technology, College of Engineering Physics, Shenzhen Technology University, Shenzhen* 518118, *China*

(Received 29 March 2024; revised manuscript received 5 June 2024; accepted manuscript online 15 June 2024)

A Wigner-distribution-like (WDL) function based on the strong-field approximation (SFA) theory is used to investigate the ionization time of the photoelectron emitted from the initial states with different magnetic quantum number m in elliptically polarized electric fields. The saddle-point method is adopted for comparisons. For different m states, a discrepancy exists in the WDL distributions of the photoelectrons emitted in a direction close to the major axis of the laser field ellipse. Based on the saddle-point analysis, this discrepancy can be ascribed to the interference between electrons ionized from two tunneling instants. Our results show that the relationships between the tunneling instants and kinetic energy of photoelectrons are the same for different m initial states when the Coulomb potential is not considered. Our work sheds some light on the ionization-time information of electrons from different magnetic quantum states.

Keywords: strong-field ionization, Wigner-distribution-like, ionization instant

PACS: 33.80.Rv, 33.80.Wz, 42.50.Hz **DOI:** 10.1088/1674-1056/ad58b3

1. Introduction

The strong-field ionization of atoms is described as electron tunneling through the potential barrier.[1] It has been found that the strong-field ionization probability in circularly polarized field depends on the electronic rotation which is determined by the initial state and can be described by the magnetic quantum number m.[2,3] Counter-rotating photoelectrons with respect to the rotation of the laser field will lead to higher ionization rate than co-rotating photoelectrons when it is in tunneling regime.[4–7] The relative helicity between the electron and laser field plays an important role in the strong-field ionization. This effect has been confirmed by both theory and experiment especially in noble gas atoms.[2,5,8–12] Recently, the sensitivity of the strong-field ionization on magnetic quantum number has been investigated in the elliptically polarized fields.[13–16] And the initial momentum at the tunnel exit has been proved to have a great influence on the instantaneous ionization rate in the elliptically polarized fields.[5,17–21]

On the other hand, it is known that the tunneling instant of the photoelectron is an important topic, for instance, the correspondence between the tunneling instant and the emission angle of the photoelectron is employed as the basis of the attoclock scheme.[14,22–25] Very recently, based on the theoretical calculations and experimental measurements, this one-to-one correspondence has been found to be broken down in the elliptically polarized fields under some special conditions.[26] Since the electrons in the initial states with different magnetic numbers have different ionization probabilities in an elliptically polarized field,[4–7,17,18,28–31] the question arises whether they have different tunneling instants. To our knowledge, there have been few relevant reports at present.

In order to answer the above question, we use a Wigner-distribution-like (WDL) function[32–34] based on the strong-field approximation (SFA) theory to investigate the time–energy distribution of the photoelectrons in elliptically polarized laser fields with different ellipticities. Then the relationships between the tunneling instant and kinetic energy of the photoelectrons can be obtained for different magnetic quantum number initial states. Moreover, our analysis shows that this relation is the same under the same laser conditions for different magnetic quantum initial states, which is qualitatively in agreement with the saddle-point result.

[†]Corresponding author. E-mail: guoli@shnu.edu.cn
[‡]Corresponding author. E-mail: zhangminzm@shnu.edu.cn
[§]Corresponding author. E-mail: chenjing@ustc.edu.cn

© 2024 Chinese Physical Society and IOP Publishing Ltd

2. Theory

The strong-field approximation theory is adopted in our work. The first term of the S-matrix element in the length gauge is given as

$$S_{\rm fi} = -{\rm i}\int_{-\infty}^{\infty} {\rm d}t \langle \chi_{\rm p}(t)|\boldsymbol{r}\cdot\boldsymbol{E}(t)|\varphi_{\rm i}(t)\rangle. \tag{1}$$

Here $\boldsymbol{r}\cdot\boldsymbol{E}(t)$ is the interaction potential between the laser field and the electron in the length gauge and $|\varphi_{\rm i}(t)\rangle = |\varphi_0\rangle {\rm e}^{{\rm i}I_{\rm p}t}$ is the atomic ground state with ionization potential $I_{\rm p}$. $\chi_{\rm p}(t)$ is the Volkov state, which is expressed by

$$|\chi_{\rm p}(t)\rangle = \frac{1}{\sqrt{v}}\exp\left\{{\rm i}[\boldsymbol{p}+\boldsymbol{A}(t)]\cdot\boldsymbol{r} - {\rm i}\int_{-\infty}^{t}\frac{[\boldsymbol{p}+\boldsymbol{A}(\tau)]^2}{2}{\rm d}\tau\right\}.$$

Here $\boldsymbol{A}(t)$ is the vector potential and the corresponding electric field $\boldsymbol{E}(t) = -\partial\boldsymbol{A}(t)/\partial t$.

To obtain the relation of ionization time and the kinetic energy of the photoelectron, the WDL function which is described in detail in Refs. [32–34] is used,

$$f\left(t,\frac{p^2}{2},\theta\right) = \frac{1}{\pi}\int_{-\infty}^{\infty} S'^{*}(t+t',\theta)S'(t-t',\theta) \times {\rm e}^{-2{\rm i}(p^2/2)t'}{\rm d}t', \tag{2}$$

where S' can be given by

$$S' = -{\rm i}\frac{\sqrt{2\pi}}{\sqrt{v}}\langle \boldsymbol{p}+\boldsymbol{A}(t)|\boldsymbol{r}\cdot\boldsymbol{E}(t)|\varphi_0\rangle \times \exp\left\{{\rm i}\int_{-\infty}^{t}\left[\boldsymbol{p}\cdot\boldsymbol{A}(\tau)+\frac{\boldsymbol{A}(\tau)^2}{2}\right]{\rm d}\tau + {\rm i}I_{\rm p}t\right\}, \tag{3}$$

where $p^2/2$ is the photoelectron kinetic energy, v is the normalization volume, and θ is the photoelectron emission angle with respect to x axis in this work, the definition of which is given in Fig. 1.

In this work, our calculations are performed for Xe atoms in elliptically polarized laser fields with a fixed peak laser intensity of 1×10^{14} W/cm^2. The ionization potential of Xe atom is 12.16 eV. The initial wave function φ_0, which is the superposition of different orbits (i.e., 3p, 4p, and 5p),[35] has a form as follows:

$$\varphi_0 = \sum_i C_i N_i r^{n_i-1}{\rm e}^{-\xi_i r}{\rm Y}_{lm}, \tag{4}$$

where the coefficients of C_i, N_i, ξ_i, and n_i are extracted from the literature.[35] ${\rm Y}_{lm}$ represents the spherical harmonic function with the orbital angular quantum number of $l=1$ and magnetic quantum numbers of $m=1$, 0, and -1. The difference of $m=1$ and $m=-1$ states is mainly from the dipole transition. Here, we take the 3p orbit of $\varphi_{3{\rm p}_\pm}(\boldsymbol{r}) = C_1N_1r^2{\rm e}^{-\xi_1 r}{\rm Y}_{1\pm1}$ in Eq. (4) as an example. And the corresponding dipole transition amplitude in Eq. (1) can be given by

$$\langle \boldsymbol{p}+\boldsymbol{A}(t)|\boldsymbol{r}\cdot\boldsymbol{E}(t)|\varphi_{3{\rm p}_\pm}(\boldsymbol{r})\rangle \propto E(t)\psi_{3{\rm p}_\pm}(\boldsymbol{p}), \tag{5}$$

where $\psi_{3{\rm p}_\pm}(\boldsymbol{p})$ is given by

$$\psi_{3{\rm p}_\pm}(\boldsymbol{p}) = \mp{\rm i}\frac{5\xi_1^2-[\boldsymbol{p}+\boldsymbol{A}(t)]^2}{\{\xi_1^2+[\boldsymbol{p}+\boldsymbol{A}(t)]^2\}^4}\sin(\phi_{\rm p}-\phi_{\rm e}){\rm e}^{\pm{\rm i}\phi_{\rm p}} + \frac{5\xi_1^4-38\xi_1^2[\boldsymbol{p}+\boldsymbol{A}(t)]^2+5[\boldsymbol{p}+\boldsymbol{A}(t)]^4}{\{[\boldsymbol{p}+\boldsymbol{A}(t)]^2+\xi_1^2\}^5} \times\cos(\phi_{\rm p}-\phi_{\rm e}){\rm e}^{\pm{\rm i}\phi_{\rm p}}. \tag{6}$$

Here, upper and lower signs of $\pm$ ($\mp$) represent the results for $m=1$ and $m=-1$ states, respectively, and $\phi_{\rm p}$ ($\phi_{\rm e}$) is the angle between the vector $\boldsymbol{p}+\boldsymbol{A}(t)$ ($\boldsymbol{E}(t)$) and the positive x axis. It can be seen that the analytical expressions of the dipole transition amplitudes of $m=\pm1$ states are complex conjugates. The same characteristics are also in the 4p and 5p states.

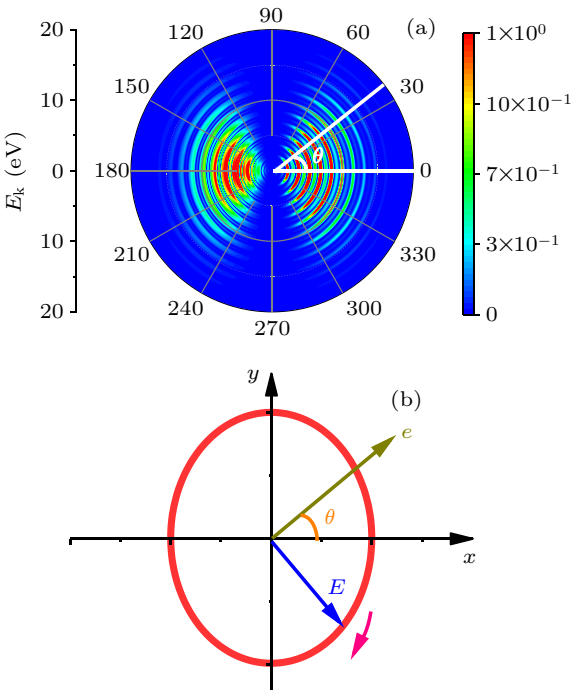


Fig. 1. (a) The angle-resolved kinetic energy distribution of photoelectrons emitted from Xe atoms in an elliptically polarized electric field with ellipticity $\varepsilon=0.6$ and $E_0=0.0535$ a.u. The major (minor) axis of the laser polarization ellipse is along the vertical (horizontal) axis. (b) The track of polarization of electric field with $\varepsilon=0.6$. θ is defined as the angle between the positive x axis and emission direction of the photoelectron. The magenta arrow indicates the rotation direction of electric field vector.

The vector potential of the laser electric field is given by

$$\boldsymbol{A}(t) = \frac{E_0}{\omega\sqrt{1+\varepsilon^2}}\sin^2\left(\frac{\omega t}{2n}\right) \times[\varepsilon\cos(\omega t)\boldsymbol{e}_x - \sin(\omega t)\boldsymbol{e}_y]. \tag{7}$$

Here, ω is the laser frequency and $n=16$ is the number of the optical cycles (o.c.) contained in the involving laser pulse.

ε and E_0 are the ellipticity and peak amplitude of the electric field. $\boldsymbol{e}_x$ and $\boldsymbol{e}_y$ are the unit vectors along the x and y axes, respectively.

For a long laser pulse with $n = 16$ o.c., the ionization characteristic is similar for each single optical cycle close to the center of the laser pulse. For clarity, the analyses based on the WDL functions and the saddle-point method only focus on the temporal range of 7.8 o.c.$< t <$ 8.5 o.c., which locates around the peak of the pulse envelop employed in our calculations. The major (minor) axis of the laser polarization ellipse is along the y axis (x axis) is presented in Fig. 1(b). And the angle-resolved kinetic energy distribution of the photoelectron in the elliptically polarized electric field described by Eq. (7) is plotted in Fig. 1(a). Atomic units (a.u.) are used unless otherwise indicated.

3. Calculations and discussion

According to Refs. [26,27], there can be two tunneling instants of the photoelectron emitted in a direction close to the minimum yield while one tunneling instant exists in the direction of the maximum yield. Therefore, we mainly focus on the photoelectrons emitted in both directions of the minimum yield (corresponding to $\theta = 90°$) and maximum yield ($\theta = 180°$) in this paper as examples.

In Fig. 2, we first give the WDL distributions of the photoelectrons ionized from Xe atomic ground states with $m = 1$ and -1 by elliptically polarized laser fields with different ellipticities at the emission angle $\theta = 90°$. The black lines denote the electron energy spectra. For comparison, the tunneling instants of the photoelectron obtained by the saddle-point method are also plotted in Fig. 2. The solution of the tunneling instants satisfies the saddle-point equation of $[\boldsymbol{p} + \boldsymbol{A}(t_s)]^2/2 = -I_p$. Here $t_s = t_0 + \mathrm{i}t_i$ is the complex time in saddle-point equation where t_0 (t_i) represents the real (image) part of the complex time. According to the saddle-point calculation, there are two tunneling instants for photoelectrons with special kinetic energies $E_k < E_c$ and these two instants merge into one when $E_k \geq E_c$. For a monochromatic laser field, the expression of E_c can be analytical given by

$$E_c = \frac{(1-\varepsilon^2)(\varepsilon^2 A_0^2 + 2I_p)}{2\varepsilon^2}, \tag{8}$$

where $A_0 = E_0/\omega\sqrt{1+\varepsilon^2}$ is the peak amplitude of laser vector potential. The detailed derivation of Eq. (8) is shown in Appendix A. In the conventional saddle-point calculations, under the same laser parameters, the correspondences between the tunneling instant and kinetic energy are the same for $m = 1$ and $m = -1$ states because the saddle-point equation is unrelated to the initial state of an atom.

As shown in Fig. 2, the WDL distributions show different structures for the laser fields with different ellipticities. In Figs. 2(a)–2(d), for relatively smaller ellipticities $\varepsilon = 0.5$ and $\varepsilon = 0.6$, two symmetric stripes corresponding to two tunneling instants are presented in the WDL distributions. The electrons emitted from these two instants with the same kinetic energy can interfere. The corresponding interference structure with positive and negative stripes appears at the vicinity of $t = 8.25$ o.c., which is consistent with the photoelectron energy spectrum (black lines). For $\varepsilon = 0.5$, the visible ionization stripes mainly focus in the lower-energy region of $E_k < 15$ eV (20 eV) for $m = 1$ ($m = -1$) state at the times deviating far from 8.25 o.c. As shown in Figs. 2(a) and 2(b), these ionization stripes qualitatively agree with the saddle-point curves, indicating that the tunneling instants in this energy region for $m = 1$ and -1 states are identical.

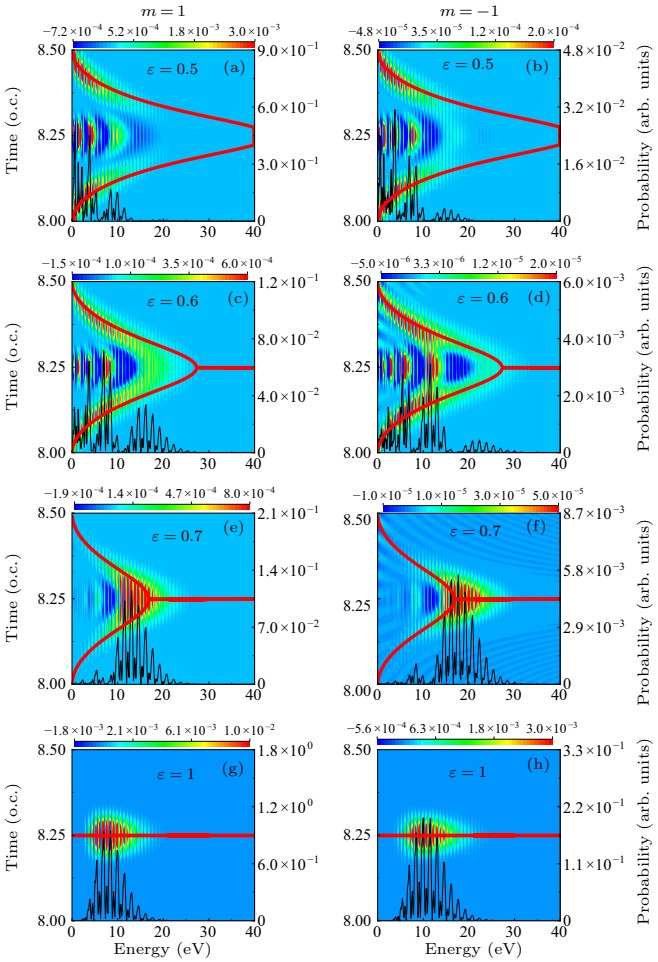


Fig. 2. The WDL distributions of the electron ionized from different magnetic quantum states of Xe atoms by 800-nm elliptically polarized laser fields with ellipticities $\varepsilon = 0.5$ [(a) and (b)], 0.6 [(c) and (d)], 0.7 [(e) and (f)], 1 [(g) and (h)] for $\theta = 90°$. The distributions in the left and right columns are for $m = 1$ and -1 states, respectively. The red solid curves denote the saddle-point solutions of Re[t_s] and the black lines represent the electron energy spectra.

When the ellipticity increases to $\varepsilon = 0.6$, the visible stripes expand to the energy of $E_k \sim 25$ eV (30 eV) for $m = 1$ ($m = -1$) state. And the ionization stripes where two tunneling instants merge into one become visible. From Figs. 2(c)

and 2(d), it seems that the saddle-point results (red lines) are in agreement with the stripes in the lower-energy region for both m states and then deviate from the stripes of $m = 1$ state with increasing kinetic energy. In other words, two ionization stripes of $m = 1$ state merge into one at $E_k \sim 16$ eV earlier than those of $m = -1$ state at $E_k \sim 24$ eV. According to our analysis, this "merging" of two ionization stripes of $m = 1$ state at $E_k \sim 16$ eV actually corresponds to the constructive interference of the photoelectrons emitted from two tunnelling instants. This can be confirmed by the energy spectra as plotted in Fig. 3 and further explanation is given below. When $\varepsilon = 0.7$, the ionization stripes in the lower-energy region of $E_k <\sim 10$ eV (12 eV) for $m = 1$ ($m = -1$) state are relatively weak, leading to very weak interference of the low-energy spectrum. Meanwhile, the visible ionization stripes mainly locate at the vicinity of $t = 8.25$ o.c. and shift to the relatively higher-energy region ranging from about 10 eV to 20 eV. Here, the WDL distributions for $m = 1$ and -1 states also exhibit a difference. This difference is ascribed to the same reason as that shown in Figs. 2(c) and 2(d). In the case of $\varepsilon = 1$, for both m states, the ionization stripes appear in the vicinity of 8.25 o.c. And the maximum value of the ionization stripe for each E_k is at time $t = 8.25$ o.c., which is consistent with the saddle-point calculations.

To shed more light on the above-mentioned difference between the WDL distributions of $m = 1$ and -1 states in the vicinity of E_c, the energy spectra are calculated by the saddle-point method and the SFA theory (i.e., numerical calculation of Eq. (1)) in logarithmic scale, respectively, in the left and right columns in Fig. 3 with the same conditions as in Fig. 2. From Fig. 3, one can find that the ionization probability from $m = 1$ state is higher than that from $m = -1$ state in the low-energy region, namely that the counter-rotating electrons with respect to the rotation of the electric field are preferred for tunneling ionization compared to the co-rotating electrons, which is in agreement with previous studies.[5,17,18] In the saddle-point calculations of Fig. 3, we consider the electrons only emitted in the temporal range of 7.8 o.c.$< t <$ 8.5 o.c. and plot the corresponding saddle-point solutions (blue lines). As shown in the left column of Fig. 3, the energy spectra in the energy region less than E_c exhibit multi-peak structures due to the interference of electrons ejected at two tunneling instants. In contrast, in the energy region $E_k > E_c$ for $\varepsilon < 1$ and whole energy region for $\varepsilon = 1$, the energy spectra show smoother curves because an electron with one tunneling instant is involved for a given E_k in these cases, resulting in no interference. Further, in the energy region close to E_c, there is a broad peak structure coming from the constructive interference for $m = 1$ state while a dip structure as marked by an arrow from the destructive interference for $m = -1$ state. According to Eq. (A10), this difference of the energy positions of the interference minima and maxima between $m = 1$ and $m = -1$ states indicates that the term of $\langle \boldsymbol{p} + \boldsymbol{A}(t_s)|\boldsymbol{r}\cdot\boldsymbol{E}(t_s)|\varphi_0\rangle$ plays an important role in the interference since the term of $e^{iS_p(t_s)}$ is independent of the magnetic quantum number m. To clearly demonstrate the interference in the energy spectrum, we plot the phase difference of the transition matrix element, i.e., equation (A10), between two saddle-point solutions for both m states in Fig. 4. As clearly shown in Fig. 4, the phase difference changes with increasing kinetic energy and is different for both states. One can find that for a given m state, the dips of the energy spectrum correspond to the energies at which the phase difference is equal to $\sim \pm\pi$. This is in accordance with the destructive interference condition. It is worthwhile to mention that an abnormal dip (spike) of the energy spectra of $m = 1$ ($m = -1$) state appears at about E_c. This is caused by the saddle-point method since there is a phase-difference jump when these two solutions are very close, which may be similar to the problem of two saddle points in the calculation of cutoff of the higher-order above-threshold ionization energy spectrum by the standard saddle-point approximation.[36] However, this does not influence our conclusion.

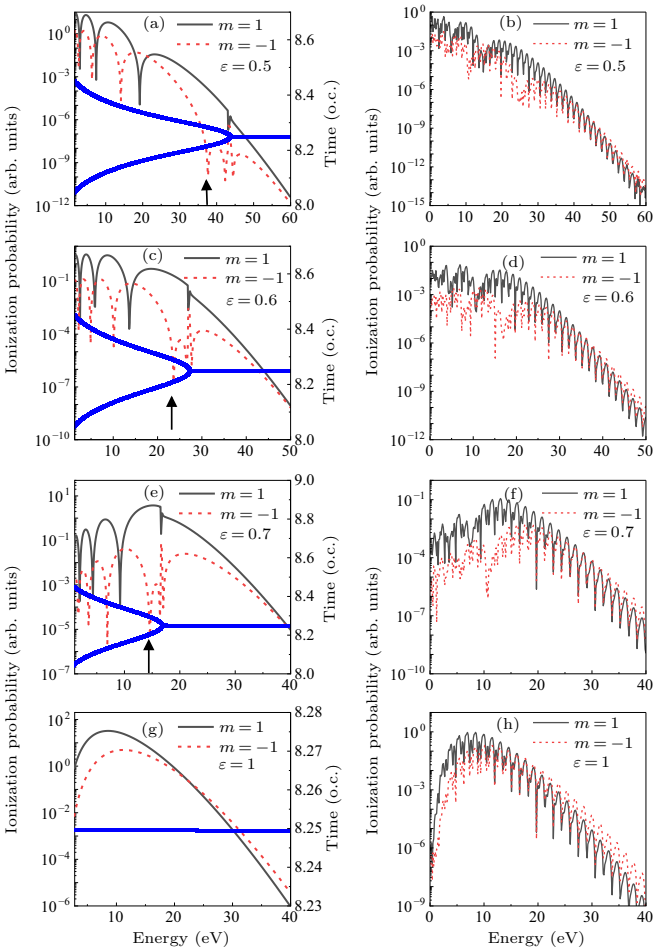


Fig. 3. The energy spectra obtained by the saddle-point method and numerical calculation of Eq. (1) in logarithmic scale in the left and right columns, respectively. The parameters are the same as in Fig. 2. The blue lines denote the saddle-point solutions.

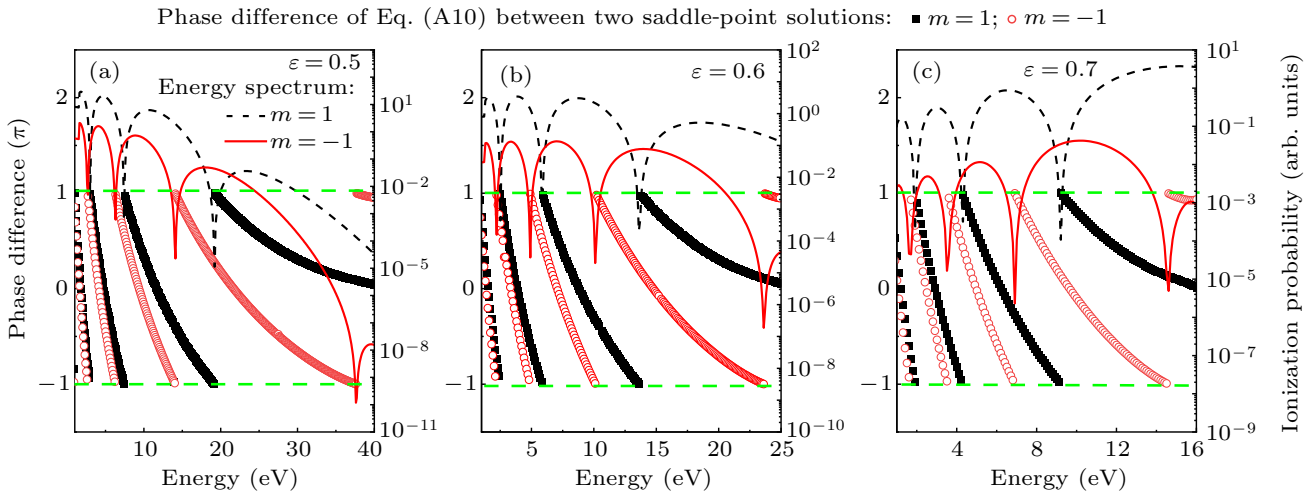


Fig. 4. The phase differences of Eq. (A10) between two saddle-point solutions in elliptically polarized fields with different ellipticities for $m=1$ and -1 states. The other parameters are the same as in Fig. 3. The short-dashed lines and solid lines represent the energy spectra obtained by the saddle-point method for $m=1$ and -1 states, respectively. The green dashed lines are given to guide the eye.

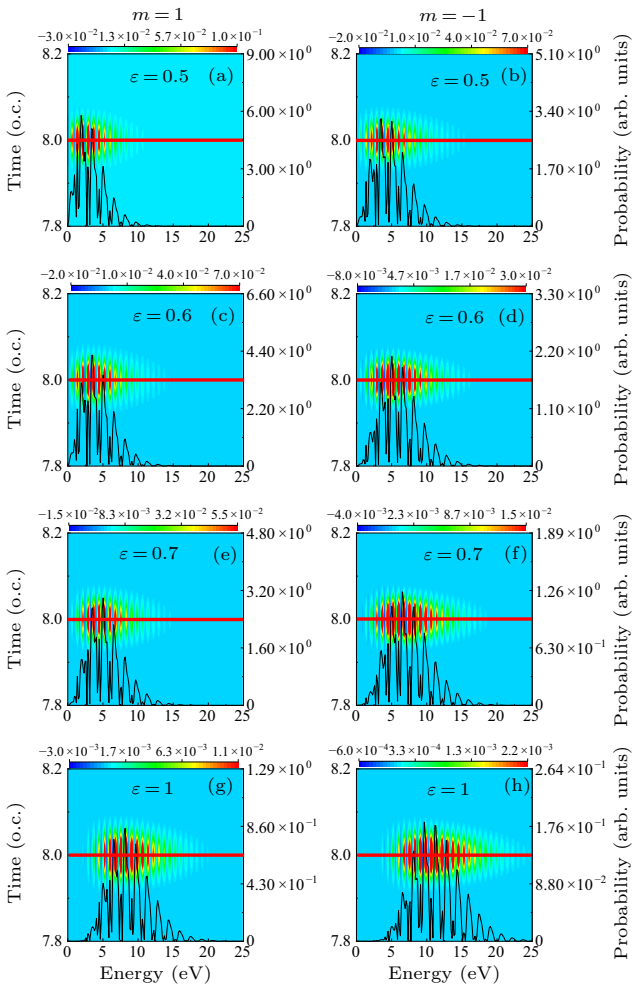


Fig. 5. The WDL distributions of photoelectrons at emission angle $\theta=180°$. The other parameters are the same as in Fig. 2. The red lines represent the saddle-point solutions and the black lines denote the energy spectra.

In the right column of Fig. 3, the energy spectra are obtained by the numerical calculations of Eq. (1). Here, we consider the electrons ionized from the whole laser pulse, which results in the regular ATI-peak structures of the energy spectra compared to the saddle-point results. By comparing the energy spectra in the left and right columns in Fig. 3, one can find that the corresponding spectra calculated by the saddle-point method and the SFA theory for the same m state are similar although there are some shifts of the positions of the peaks (dips) of the energy spectra when $\varepsilon<1$. For example, for $m=1$ state, one broad peak structure in the vicinity of $E_k\sim16$ eV in Fig. 3(d) corresponds to the structure in the vicinity of $E_k\sim17$ eV in Fig. 3(c), which results from the interference enhancement. This indicates that the "merging" of two ionization stripes presented in Fig. 2(c) in the vicinity of $E_k\sim16$ eV actually corresponds to the interference structure where two tunneling instants remain. The similar scenario also occurs in the case of $\varepsilon=0.7$.

Due to the fact that the tunneling instant is dependent of the emission angle of the electron in an elliptically polarized electric field, the WDL distributions of the electrons at $\theta=180°$ are also presented in Fig. 5 with the same laser parameters as those in Fig. 2. In contrast to Fig. 2, all the ionization stripes focus at the vicinity of $t=8$ o.c. regardless of the ellipticity. More precisely, the maximum ionization probability at each E_k exactly corresponds to the time of $t=8$ o.c. at which the instantaneous electric field is along the major axis of the laser polarization ellipse. The energy spectra (black lines) show regular ATI-peak structures, which are totally different from the multi-peak structures shown in Figs. 2(a)–2(d) originating from the interference between the electrons emitted from two tunneling instants. The above-mentioned features mean that there is only one tunneling instant in this case, which is well consistent with the saddle-point results (horizontal lines). It can be concluded that the tunneling instants are

the same for these two different m states when the ionization occurs when the laser field reaches the maximum.

For a comprehensive understanding on the characteristics of photoelectrons from different magnetic quantum number states, we also calculate the WDL distributions of photoelectron from $m = 0$ state although its contribution is negligible compared to the other two states in an elliptically polarized field. It is known that there is no electron distribution for $m = 0$ state in the x–y plane, i.e., the plane of the laser field polarization considered in this paper. Therefore in the calculation of $m = 0$ state, we focus on the photoelectrons emitted along a direction in the polar angle of 85° between the emission angle and the positive z axis and the azimuthal angles of $\theta = 90°$ and $\theta = 180°$ as defined in Fig. 1. The WDL distributions for $m = 0$ state are plotted in Fig. 6 with the same laser parameters as those in Fig. 2, which are similar to the corresponding distributions of $m = 1$ and -1 states as presented in Figs. 2 and 5.

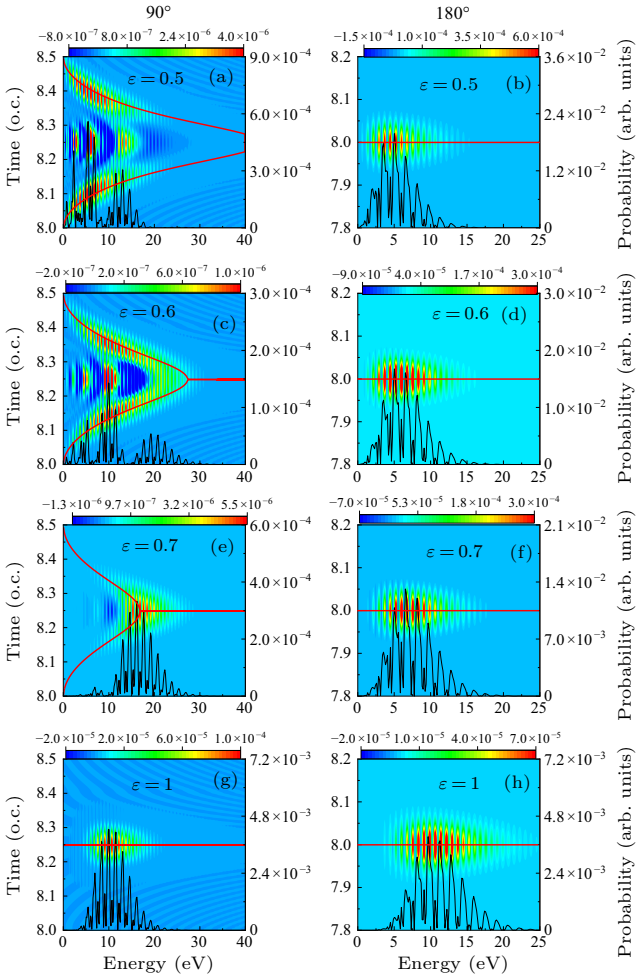


Fig. 6. The WDL distributions of photoelectrons from $m = 0$ state ejected along the direction in the polar angle of 85° and the azimuthal angle of $\theta = 90°$ (left column) and $\theta = 180°$ (right column). The other parameters are the same as in Figs. 2 and 5. The red lines represent the saddle-point solutions and the black lines denote the energy spectra.

From Figs. 2, 5, and 6, it can be concluded that when the Coulomb potential is not considered the ionization times of photoelectrons emitted from different m states are the same under the same laser conditions, which are independent of the helicity of the initial-state electron with respect to the rotation of the electric field vector.

Furthermore, we investigate the wavelength dependence of the WDL distribution for different magnetic quantum number states. In Fig. 7, the WDL distributions of photoelectrons ionized from different initial states at $\theta = 90°$ are given in the elliptically polarized laser fields with $\varepsilon = 0.6$ for different wavelengths 400 nm [Figs. 7(a)–7(c)] and 1200 nm [Figs. 7(g)–7(i)]. For comparison, the corresponding WDL distributions for 800 nm discussed above are also presented. In the case of 400 nm, although the photoionization belongs to the multi-photon regime, two symmetric broad ionization stripes, together with the corresponding interference structure appearing at the vicinity of $t = 8.25$ o.c., are still visible in the WDL distributions. This indicates that two ionization instants for special energy $E_k < E_c$ can be approximately satisfied, which are also in agreement with the saddle-point results. When the wavelength of the electric field varies, the changes of the WDL distributions for three magnetic quantum number states follow the same tendency. From Fig. 7, one can find that in one given wavelength case, the ionization stripes in the WDL distributions of $m = 1$, 0, and -1 states are qualitatively consistent with each others except for the interference structures originating from two tunneling instants. In addition, for $\theta = 180°$ in the cases of 400 nm and 1200 nm, the ionization stripes of $m = 1$, 0, and -1 states also mainly focus at the vicinity of $t = 8$ o.c. (not shown here), indicating that the ionization times are the same for different magnetic quantum states.

From Fig. 7, we can find that for the same m, the energy of the peak of the WDL distribution gets closer to E_c with increasing wavelength. In order to explain this reason, we calculate the relationship between the energy and emission angle of electrons by the semiclassical relation of $\boldsymbol{p} = -\boldsymbol{A}(t)$ in Fig. 8. As shown in Fig. 8, when the wavelength is 400 nm (800 nm, 1200 nm), the energy of the electrons emitted from the angle of $\theta = 90°$ is 2.2 eV (8.8 eV, 20 eV), which is qualitatively consistent with the energy corresponding to the maximum WDL distribution. This is in accordance with the understanding that the electrons with highest yields usually have zero velocity after tunneling under the adiabatic condition. Furthermore, compared with the corresponding E_c, it is obvious that the above-mentioned energies are closer to E_c with increasing wavelength, which actually indicates the ionization features in the tunneling regime.

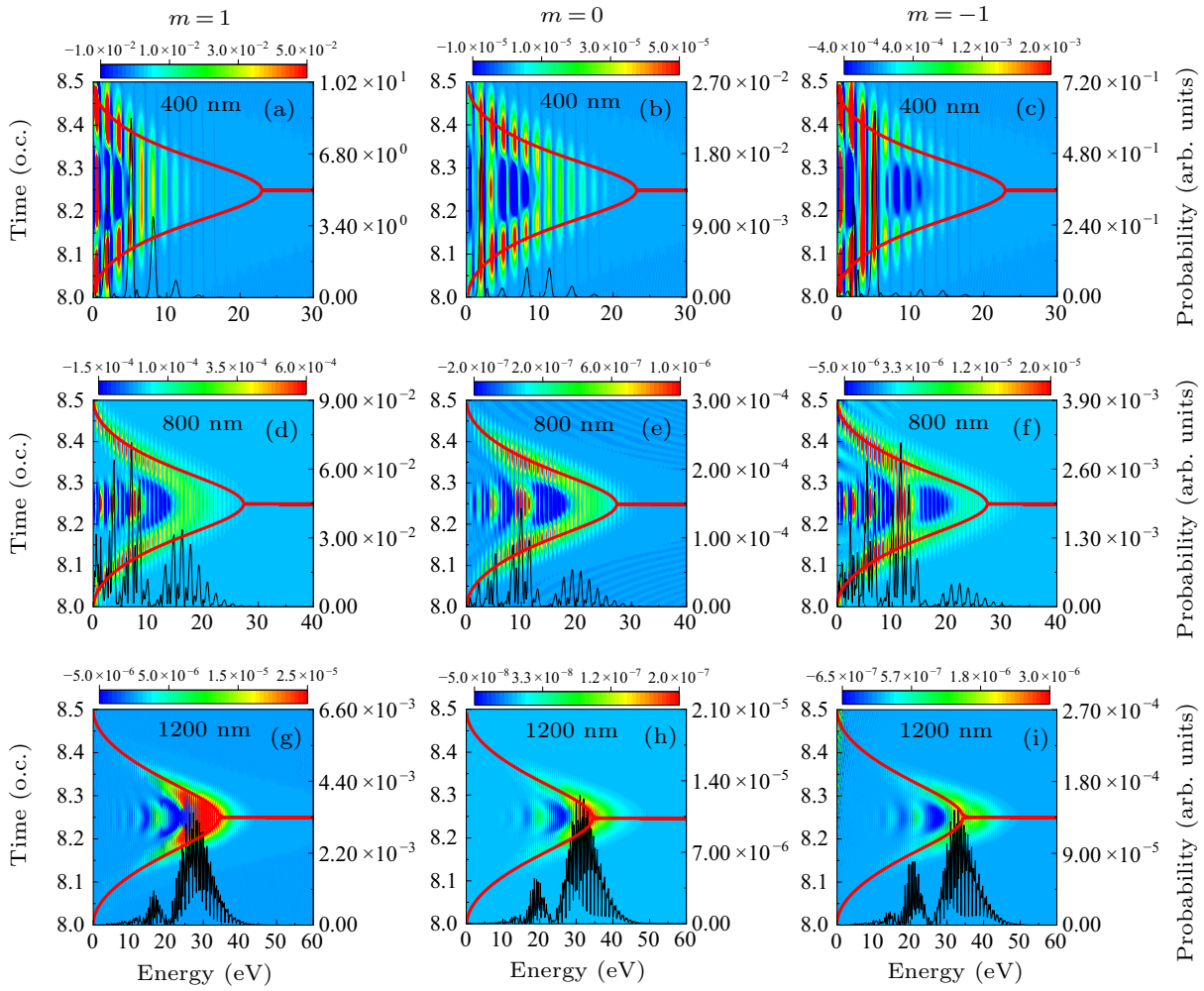


Fig. 7. The WDL distributions at the emission angle $\theta = 90°$ in the laser electric field with ellipticity $\varepsilon = 0.6$ for different wavelengths 400 nm [(a)–(c)], 800 nm [(d)–(f)], and 1200 nm [(g)–(i)]. The red lines represent the saddle-point solutions and the black lines represent the energy spectra.

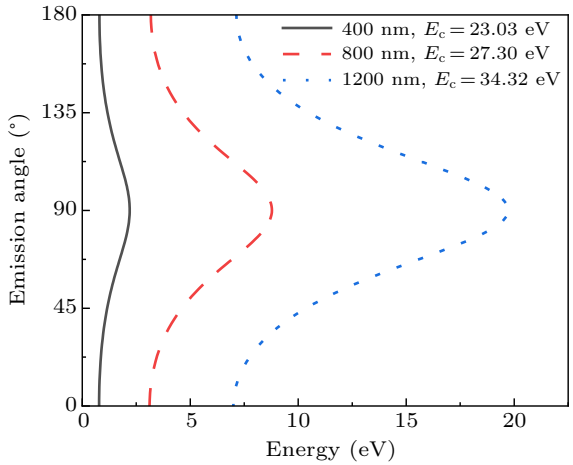


Fig. 8. The relationships between the energy and emission angle of photoelectrons obtained by semi-classical method for three different wavelengths (400 nm, 800 nm, and 1200 nm). The corresponding E_c is also given in the panel. The parameters are the same as in Fig. 7.

4. Conclusion

We use the Winger-distribution-like function based on the SFA theory to calculate the time–energy distribution of photoelectron ionized from initial p orbital with different magnetic quantum numbers in elliptically polarized electric fields. When the photoelectron is emitted along the direction of the major axis of the laser polarization ellipse, there is a difference between the WDL distributions of different m states in the energy region close to the critical energy where two tunneling instants merge into one. According to saddle-point analysis, this difference can be attributed to the interference between electrons emitted from two tunneling instants. In this case, the relation between the tunneling instant and the emission angle for different m states is identical. When the electron is emitted along the direction of the minor axis of the polarization ellipse, the ionization time corresponding to the maximum of the electric field is not only the same for different magnetic quantum states but also well consistent with the saddle-point results. Our study sheds some light on the tunneling instant of electrons emitted from different magnetic quantum number states.

Appendix A: Saddle-point solution for emission angle of 90°

For the emission angle of $\theta = 90°$, the components of the momentum are $p_x = 0$ and $p_y = \sqrt{2E_k}$. For simplicity, the

vector potential of a monochromatic laser field is employed, whose components along x and y axis are $A_x = A_0\varepsilon\cos\omega t$ and $A_y = -A_0\sin\omega t$, respectively. Here $A_0 = E_0/\omega\sqrt{1+\varepsilon^2}$ is the amplitude of laser vector potential.

One can substitute the complex time $t_s = t_0 + \mathrm{i}t_\mathrm{i}$ into the saddle-point equation of $[\boldsymbol{p}+\boldsymbol{A}(t)]^2 + 2I_\mathrm{p} = 0$. Then both real and image parts of the saddle-point equation can be given as follows.

The real part of saddle-point equation satisfies

$$\begin{aligned}&(p_y - A_0\sin\omega t_0\cosh\omega t_\mathrm{i})^2 - A_0^2\cos^2\omega t_0\sinh^2\omega t_\mathrm{i}\\&\quad+\varepsilon^2A_0^2(\cos^2\omega t_0\cosh^2\omega t_\mathrm{i} - \sin^2\omega t_0\sinh^2\omega t_\mathrm{i})\\&\quad+2I_\mathrm{p} = 0.\end{aligned}\tag{A1}$$

The image part of saddle-point equation satisfies

$$\begin{aligned}&(p_y - A_0\sin\omega t_0\cosh\omega t_\mathrm{i})A_0\cos\omega t_0\sinh\omega t_i\\&\quad+\varepsilon^2A_0^2\cos\omega t_0\cosh\omega t_\mathrm{i}\sin\omega t_0\sinh\omega t_\mathrm{i} = 0.\end{aligned}\tag{A2}$$

If $\cos\omega t_0 \neq 0$, equation (A2) is rewritten as

$$\cosh\omega t_\mathrm{i} = \frac{p_y}{(1-\varepsilon^2)A_0\sin\omega t_0}.\tag{A3}$$

Combined with Eqs. (A1) and (A3), we can obtain

$$\begin{aligned}&-A_0^2(1-\varepsilon^2)^2\sin^4\omega t_0 + [(A_0^2+2I_\mathrm{p})(1-\varepsilon^2)\\&\quad+(1-\varepsilon^2)p_y^2]\sin^2\omega t_0 - p_y^2 = 0.\end{aligned}\tag{A4}$$

By solving Eq. (A4), we can get

$$\sin^2\omega t_0 = \frac{-(A_0^2+2I_\mathrm{p}+2E_\mathrm{k}) + \sqrt{(A_0^2+2I_\mathrm{p}+2E_\mathrm{k})^2 - 8A_0^2E_\mathrm{k}}}{-2A_0^2(1-\varepsilon^2)}.\tag{A5}$$

Obviously, for a given E_k, equation (A5) has two solutions of t_0 in each half optical cycle because of $\sin^2\omega t_0 < 1$. When t_0 is given, the image time t_i can also be determined by Eq. (A3).

Accordingly, the right-hand of Eq. (A5) should be less than 1. Then the below condition is obtained:

$$E_\mathrm{k} < \frac{(1-\varepsilon^2)(\varepsilon^2A_0^2+2I_\mathrm{p})}{2\varepsilon^2}.\tag{A6}$$

If $\cos\omega t_0 = 0$, then $\sin\omega t_0 = 1$ in this work. Under this condition, equation (A1) can be simplified as

$$\begin{aligned}&(1-\varepsilon^2)A_0^2\cosh^2\omega t_\mathrm{i} - 2p_yA_0\cosh\omega t_\mathrm{i}\\&\quad+p_y^2+\varepsilon^2A_0^2+2I_\mathrm{p} = 0.\end{aligned}\tag{A7}$$

In order to obtain real solutions of above equation, the inequality should be satisfied as follows:

$$p_y^2 - (1-\varepsilon^2)(p_y^2+\varepsilon^2A_0^2+2I_\mathrm{p}) \geq 0.\tag{A8}$$

Substituting $p_y = \sqrt{2E_\mathrm{k}}$ into Eq. (A6), we have

$$E_\mathrm{k} \geq \frac{(1-\varepsilon^2)(\varepsilon^2A_0^2+2I_\mathrm{p})}{2\varepsilon^2}.\tag{A9}$$

One critical energy $E_\mathrm{c} = (1-\varepsilon^2)(\varepsilon^2A_0^2+2I_\mathrm{p})/2\varepsilon^2$ is set. Based on above analysis, it can be found that there are two tunneling instants when $E_\mathrm{k} < E_\mathrm{c}$, while only one tunneling instant exists when $E_\mathrm{k} \geq E_\mathrm{c}$ within half an optical cycle.

Further, we apply the saddle-point approximation to Eq. (1) to carry out the integration over time. The transition matrix element is given as follows:

$$\begin{aligned}S_\mathrm{fi}^\mathrm{SP} = -\mathrm{i}\sum_s\left\{\frac{2\pi\mathrm{i}}{\boldsymbol{E}(t_s)\cdot[\boldsymbol{p}+\boldsymbol{A}(t_s)]}\right\}^{1/2}\\\times\langle\boldsymbol{p}+\boldsymbol{A}(t_s)|\boldsymbol{r}\cdot\boldsymbol{E}(t_s)|\varphi_0\rangle\,\mathrm{e}^{\mathrm{i}S_{\boldsymbol{p}}(t_s)}.\end{aligned}\tag{A10}$$

Here, the action $S_\mathrm{p}(t_s) = \int_{-\infty}^{t_s}[\boldsymbol{p}+\boldsymbol{A}(\tau)]^2/2\,\mathrm{d}\tau + I_\mathrm{p}t_s$ and s denotes the number of the saddle-point solution.

Acknowledgements

We thank W. Quan for helpful discussion. Project supported by the National Key Research and Development Program of China (Grant No. 2019YFA0307700) and the National Natural Science Foundation of China (Grant Nos. 12274300 and 12074261)

References

[1] Reiss H R 1980 *Phys. Rev. A* **22** 1786
[2] Herath T, Yan L, Lee S K and Li W 2012 *Phys. Rev. Lett.* **109** 043004
[3] Gajda M, Piraux B and Rzażewski K 1994 *Phys. Rev. A* **50** 2528
[4] Barth I and Smirnova O 2011 *Phys. Rev. A* **84** 063415
[5] Eckart S, Kunitski M, Richter M, Hartung A, Rist J, Trinter F, Fehre K, Schlott N, Henrichs K, Schmidt L P H, Jahnke T, Scöffler M, Liu K L, Barth I, Kaushal J, Morales F, Ivanov M, Smirnova O and Dörner R 2018 *Nat. Phys.* **14** 701
[6] Li Y, Lan P F, Xie H, He M R, Zhu X S, Zhang Q B and Lu P X 2015 *Opt. Express* **23** 028801
[7] Barth I and Lein M 2014 *J. Phys. B: At. Mol. Opt. Phys.* **47** 204016
[8] Beiser S, Klaiber M and Kiyan I Y 2004 *Phys. Rev. A* **70** 011402
[9] Barth I and Smirnova O 2013 *Phys. Rev. A* **87** 065401
[10] Rey H F and van der Hart H W 2014 *Phys. Rev. A* **90** 033402
[11] Patchkovskii S, Vrakking M J J, Villeneuve D M and Niikura H 2020 *J. Phys. B: At. Mol. Opt. Phys.* **53** 134002
[12] Wang R R, Ma M Y, Wen L C, Guan Z, Yang Z Q, Jiao Z H, Wang G L and Zhao S F 2023 *J. Opt. Soc. Am. B* **40** 1749
[13] Liu K, Ni H C, Renziehausen K, Rost J M and Barth I 2018 *Phys. Rev. Lett.* **121** 203201
[14] Torlina L, Morales F, Kaushal J, Ivanov I, Kheifets A, Zielinski A, Scrinzi A, Muller H G, Sukiasyan S, Ivanov M and Smirnova O 2015 *Nat. Phys.* **11** 503
[15] Walker S , Kolanz L, Venzke J and Becker A 2021 *Phys. Rev. Research* **3** 043051
[16] Walker S , Kolanz L, Venzke J and Becker A 2021 *Phys. Rev. A* **103** L061101
[17] Barth I and Smirnova O 2013 *Phys. Rev. A* **88** 013401
[18] Barth I and Smirnova O 2013 *Phys. Rev. A* **87** 013433
[19] Luo S Q, Li M, Xie W H, Liu K, Feng Y D, Du B J, Zhou Y M and Lu P X 2019 *Phys. Rev. A* **99** 053422
[20] Ivanov I A 2016 *Phys. Rev. A* **93** 053403
[21] Yuan M H and Bian X B 2015 *Phys. Rev. A* **101** 013412
[22] Lin Z Y, Lin B Q and Chen Z X 2018 *Acta Optica Sinica* **38(6)** 0602001
[23] Eckle P, Pfeiffer A N, Cirelli C, Staudte A, Diiörner R, Muller H G, Biiüttiker M and Keller U 2008 *Science* **322** 1525

[24] Han M, Ge P P, Wang J G, Guo Z N, Fang Y Q, Ma X Y, Yu X Y, Deng Y K, Wörner H J, Gong Q H and Liu Y Q 2021 *Nat. Photon.* **15** 765
[25] Yu M, Liu K, Li M, Yan J Q, Cao C P, Tan J, Liang J T, Guo K Y, Cao W, Lan P F, Zhang Q B, Zhou Y M and Lu P X 2022 *Light: Sci. Appl.* **11** 215
[26] Guo L, Zhao M, Quan W, Liu X J and Chen J 2023 *Optica* **10** 1316
[27] Liu M M, Shao Y, Han M, Ge P P, Deng Y, Wu C Y, Gong Q H and Liu Y Q 2018 *Phys. Rev. Lett.* **120** 043201
[28] Trabert D, Hartung A, Eckart S, Trinter F, Kalinin A, Schöffler M, Schmidt L Ph H, Jahnke T, Kunitski M and Dörner R 2018 *Phys. Rev. Lett.* **120** 043202
[29] Wen L C, Jing W Q, Sun C P, Gao X H, Jiao Z H, Wang G L, Chen J H and Zhao S F 2023 *J. Phys. B: At. Mol. Opt. Phys.* **56** 125601
[30] Xu S L, Zhang Q B, Fu X L, Huang X, Han X, Li M, Cao W and Lu P X 2020 *Phys. Rev. A* **102** 063128
[31] Serebryannikov E E and Zheltikov A M 2016 *Phys. Rev. Lett.* **116** 123901
[32] Guo L, Han S S and Chen J 2010 *Opt. Express* **18** 1240
[33] Guo L, Han S S and Chen J 2012 *Phys. Rev. A* **86** 053409
[34] Guo L, Chen S, Hu S L, Lu R H, Han S S, Zhang J T and Chen J 2022 *J. Phys. B: At. Mol. Opt. Phys.* **55** 225401
[35] Radzig A A and Smirnov B M 1985 *Reference Data on Atoms, Molecules and Ions*
[36] Figueira de Morisson Faria C, Schomerus H and Becker W 2002 *Phys. Rev. A* **66** 043413